J Nanopart Res (2020) 22:216
https://doi.org/10.1007/s11051-020-04944-1

RESEARCH PAPER

Selective uptake of Ag(I) from aqueous solutions using ionic liquid-modified iron oxide nanoparticles

Abiodun D. Aderibigbe · Richard A. Crane · Martin R. Lees · Andrew J. Clark

Received: 5 March 2020 / Accepted: 1 July 2020

Abstract Surface functionalized magnetic nanoparticles represent a potentially highly valuable new suite of technologies for the selective recovery of metals from the aqueous phase, due to their ability to be manipulated and then recovered using an externally applied magnetic field. Ionic liquids are ideal candidates for such surface functionalization for a range of reasons, including their enhanced selectivity, low water consumption, and high chemical stability. Herein the removal of Ag^+ onto $[MTESPIm]^+[Cl]^-$ on $Fe_3O_4@SiO_2$ has been investigated as a function of pH, exposure time, nanosorbent concentration, and type of stripping agent. The Ag^+ removal was recorded to fit the Langmuir isotherm indicating monolayer formation, with a saturation capacity of 23.69 mg/g. Optimum conditions for the selective removal of Ag^+ in preference to Cu^{2+} and Pb^{2+} were recorded at pH 3, exposure time ranging between 0 and 15 min, and at the highest nanosorbent dose tested (80 mg nanosorbent/10 mL of adsorbate solution) Moreover, thiourea outperformed both HNO_3 and HCl for the stripping of sorbed Ag^+, with optimum efficacy at 0.6 M. Overall, the results indicate that $[MTESPIm]^+[Cl]^-$ on $Fe_3O_4@SiO_2$ is a highly adaptable and efficient agent for the selective recovery of Ag from the aqueous phase.

Keywords Selective silver recovery · Ionic liquid · Iron oxide nanoparticle · Surface functionalization · Soft donor

A. D. Aderibigbe (✉) · A. J. Clark
Department of Chemistry, University of Warwick, Coventry CV4 7AL, UK
e-mail: a.aderibigbe.1@warwick.ac.uk

R. A. Crane
Camborne School of Mines, College of Engineering, Mathematics and Physical Sciences, University of Exeter, Penryn Campus, Penryn, Cornwall TR10 9FE, UK

R. A. Crane
Environment and Sustainability Institute, University of Exeter, Penryn Campus, Penryn, Cornwall TR10 9FE, UK

M. R. Lees
Department of Physics, University of Warwick, Coventry CV4 7AL, UK

Present Address:
A. D. Aderibigbe
Chemistry Department, Federal University of Technology Akure, P.M.B. 704, Akure, Ondo State, Nigeria

Introduction

As the global population continues to expand, demand for modern products and services which use silver (Ag), including electronic equipment, catalysis, antibacterial agents, jewelry, water filtration media, etc., will almost certainly continue to increase (Sahan et al. 2019; Taillades and Sarradin 2004; Butterman and Hilliard 2005). Moreover, Ag is listed within the EU 27 critical raw materials, and currently exhibits an "end-of-life recycling input rate" of only ~14% (Butterman and Hilliard 2005). Therefore, in order to overcome this

Published online: 19 July 2020

urgent and burgeoning problem, new technology is required for the enhanced recovery of Ag from our waste materials and end-of-life products (Avarmaa et al. 2019). A key challenge associated with this, however, is that such waste is typically chemically complex and mixed with a wide range of ancillary metal(loids)/materials. It is therefore clear that the development of increasingly efficient, selective and cost-effective Ag^+ recovery process is highly beneficial.

To date, much research and development has been conducted on the removal of Ag ions from the aqueous phase including solvent extraction (Daubinet and Kaye 2002), ion exchange (Virolainen et al. 2015), chemical precipitation (Ahlatcı et al. 2016), and solid phase extraction (Abdolmohammad-Zadeh and Javan 2015; Karimi et al. 2012). Solid phase removal media have often been preferred due to the simplicity of their application, their often low disposal costs, and often high removal efficacy (Abdolmohammad-Zadeh and Javan 2015). Within such applications, nanoparticles, defined as particles which exhibit at least one length < 100 nm, have received great interest due to their superior surface area and commensurate high reactivity with the aqueous phase. Such materials are also able to be suspended in the aqueous phase as a stable colloid and can therefore be utilized in various next-generation applications involving in situ subsurface metal immobilization or recovery (Crane and Scott 2012). Magnetic nanoparticles have also received particularly high interest due to their additional ability to be manipulated and then recovered from the aqueous phase using an externally applied magnetic field (Dupont et al. 2014; Filippousi et al. 2014; Hufschmid et al. 2015). Additional important properties for nanosorbents include stability across a wide pH range, high and rapid ion extraction efficacy, facile ion stripping efficacy, and low synthesis cost (Crane et al. 2019). In recent years, a number of studies have emerged on the development of such nanotechnology for Ag removal from the aqueous phase. For example, Jalilian and Taheri (2018) reported that nanoscale Fe_3O_4@SiO_2@TiO_2@ Ag^+-imprinted 2,4-diamine-6-phenyl-1,3,5-triazine demonstrated a higher distribution ratio and selectivity coefficient than the non-imprinted analogue in the selective extraction and preconcentration of Ag^+. Extraction efficiency, however, was reported to significantly diminish at pH 3. The synthesis of a Ag^+ imprinted 3-(triethoxysilyl)propane-1-thiol tethered to Fe_3O_4@SiO_2@TiO_2 was reported and it was determined that the nanosorbent exhibits relatively high selectivity, at room temperature, for Ag^+ from aqueous solutions also containing Li^+, Co^{2+}, Cu^{2+}, and Ni^{2+} (Yin et al. 2017). While this work has been proven as successful at bench scale, its efficacy for industrial scale application remains largely unquantified and research on this topic (and in particular on the use of low-cost reagents and industrially scalable processes) is currently lacking. In a separate study, the combination of 5-amino-2-thiol-1,3,4-thiadiazole and sodium dodecyl sulphate tethered by their condensation onto Fe_3O_4/Al_2O_3, was reported to extract Ag^+ selectively, rapidly and quantitatively even in the presence of several order of magnitude greater concentrations of Zn^{2+}, Bi^{3+} and Pd^{2+} (Karimi et al. 2012). Finally, the nanosorbent Fe_3O_4@SiO_2@(1*E*,1′*E*)-1,1′-(pentane-1,5-diylbis(2,1-phenylene))bis(*N*-(3-(trimethoxysilyl)propyl)methanimine) was recorded to selectively remove Ag^+ in preference to Pb^{2+} and Cu^{2+} (Banaei et al. 2015).

Ionic liquids (ILs) are defined as compounds which are entirely ionic. Such chemicals therefore often exhibit unique properties including little or very low volatility, low melting point, thermal stability, and tunable hydrophilicity/hydrophobicity (Zhou et al. 2012; Seddon et al. 2000). For example, 1-methyl-3-[(3-trimethoxysilyl)propyl] imidazolium chloride ($[MTMSPIm]^+[Cl]^-$) was anchored onto Mn_3O_4@SiO_2 nanoparticles and observed to demonstrate high selectivity, reusability, and efficiency for extraction and preconcentration of ultratrace concentrations of Ag+ (i.e., 60 ng/mL) (Abdolmohammad-Zadeh and Javan 2015). A key shortcoming, however, was that the nanosorbent was also not ideally suited for magnetic recovery applications due to the significantly lower magnetization saturation of Mn_3O_4 compared with Fe_3O_4 (Ozkaya et al. 2008).

Herein we have built on the work of Abdolmohammad-Zadeh and Javan (2015) by combining the proven selectivity of the ionic liquid $[MTESPIm]^+[Cl]^-$ for Ag^+ recovery with the superior magnetic responsiveness of Fe_3O_4@SiO_2. While Fe_3O_4@SiO_2@$[MTESPIm]^+[Cl]^-$ (Fig. 1) has been applied in various different applications to date (e.g., catalysis, medicine, printing (Qian et al. 2017; Sajjadifar et al. 2019; Yang et al. 2011; Wei et al. 2013; Azgomi and Mokhtary 2015; Garkoti et al. 2017; Zhou et al. 2012)), to the best of our knowledge, this is the first study which has investigated its potential application for Ag^+ uptake. The aim of this work was therefore to investigate the behavior of Fe_3O_4@SiO_2@$[MTESPIm]^+[Cl]^-$ towards

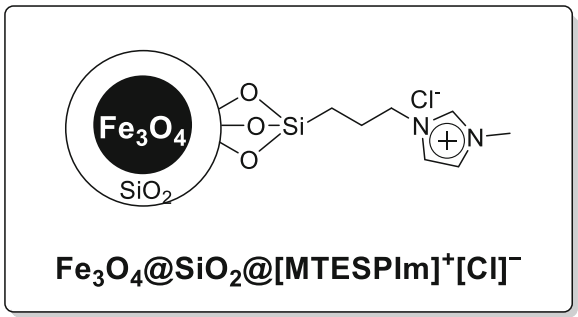

Fig. 1 Core-shell iron oxide/imidazolium-based ionic liquid composite nanosorbent (Fe_3O_4@SiO_2@$[MTESPIm]^+[Cl]^-$)

Ag^+ across a range of fundamental constraints (namely, pH, contact time, nanosorbent dose, Ag^+ recovery efficacy by different stripping agents) in order to understand Ag^+ removal kinetics and mechanisms and thereby determine optimal application conditions.

Experimental details

Chemicals

$FeSO_4.7H_2O$ (99%), $FeCl_3.6H_2O$ (97%), NH_4OH (25% *v*/v), tetraethyl orthosilicate (99%), *N*-methylimidazole (99%), 3-Chloropropyltriethoxysilane (97%), thiourea (99%), and toluene (99.5%) were purchased from Sigma Aldrich. HCl (37%), HNO_3 (70%), $AgNO_3$ (99%), $NaNO_3$ (99%), and NaOH pellets (97%) were purchased from Fisher Scientific. $Cu(NO_3)_2.3H_2O$ (99%) and $Pb(NO_3)_2$ (99%) were purchased from Acros Chemicals. Ethanol absolute (99.8%) was purchased from VWR. All chemicals were used as received without further purification.

Equipment and characterization

All ^1H and ^{13}C NMR spectra were recorded at room temperature on Bruker Advance spectrometers. Fourier transform infra-red (FTIR) spectra were recorded on Bruker Alpha Platinum-Attenuated Total Reflectance IR spectrometer. X-ray diffraction (XRD) data were collected on a Panalytical Empyrean X-ray diffractometer employing a Co Kα radiation at 40 kV and 40 mA. Transmission electron micrographs were captured by means of the JEOL 2100+ machine operating an acceleration voltage of 200 kV from samples prepared on a copper EM grid. X-ray photoelectron spectroscopy (XPS) data were collected on the Kratos AXIS Ultra DLD spectrometer and take off angle of 90° was used with Al(mono) X-ray source. Metal concentrations were measured by means of a PerkinElmer 5300DV Inductively Coupled Plasma Optical Emission spectrophotometer (ICP-OES). Thermogravimetry analyses (TGA) were undertaken by means of a Metler Toledo DSC1-STAR at a scan rate of 10 °C/min on samples placed inside 70-μL alumina pans under a nitrogen atmosphere from 25 to 900 °C. Magnetization versus field data were recorded on a Quantum Design MPMS 5S SQUID magnetometer at 300 K. Finally, the pH of

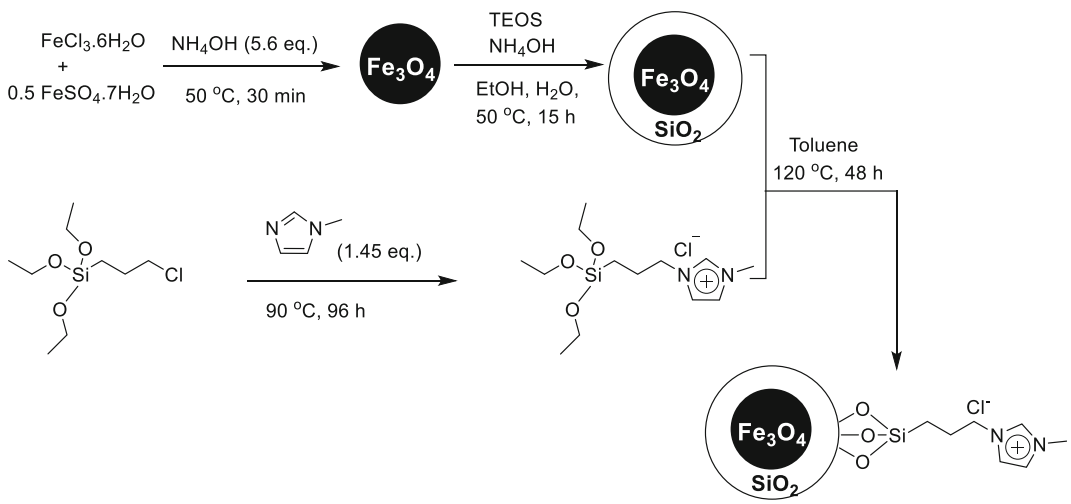

Scheme 1 Schematic diagram depicting the stepwise synthesis of $[MTESPIm]^+$ $[Cl]^-$ on Fe_3O_4@SiO_2

the adsorbate solutions was monitored using the Hanna HI 8424 portable pH meter.

Synthesis of the ionic liquid immobilized on silica-coated Fe_3O_4 nanoparticles

The synthesis of the ionic liquid-modified silica-coated Fe_3O_4 nanosorbent was achieved over four steps (Scheme 1). In the first step, the magnetic core (nanoscale Fe_3O_4) was prepared following Naka et al. (2008). Briefly, $FeCl_3.6H_2O$ (5.41 g, 0.02 mol) and $FeSO_4.7H_2O$ (2.78 g, 0.01 mol) were dissolved by stirring in deionized H_2O (300 mL) at 50 °C and under a nitrogen atmosphere. NH_4OH (8.52 mL, 13.20 M, 0.11 mol) was then added to the iron salts solution and stirred at 1200 rpm for 30 min. The resultant black precipitates were then separated from the aqueous phase using an externally applied magnetic field. The solids were then washed with H_2O (100 mL × 3) and ethanol (50 mL × 3). The nanoscale Fe_3O_4 solids were then dried at approximately 300 mbar at 70 °C for 2 h. The SiO_2 coating was prepared following the method reported by Fan et al. (2016). Briefly, to a stirred suspension of Fe_3O_4 (0.4 g) and TEOS (0.36 g) in dry ethanol (3 mL) at 50 °C was added a mixture of NH_4OH (0.66 mL, 13.20 M), ethanol (1.2 mL), and H_2O (0.58 mL). The reaction was left to stir for 8 h at 50 °C under a nitrogen atmosphere and at the end of which the product suspension was left to cool to room temperature. The solids obtained were separated with an externally applied magnetic field, washed with H_2O (25 mL × 3), and finally dried at 300 mbar and 70 °C to give Fe_3O_4@SiO_2 as a black solid. In the next step, the ionic liquid, 1-methyl-3-[(3-triethoxysilyl)propyl] imidazolium chloride ($[MTESPIm]^+[Cl]^-$), was accessed following a protocol previously reported by Abdolmohammad-Zadeh and Javan (2015). Hence, a mixture of N-methylimidazole (4.8 mL, 0.06 mol) and 3-chloropropyltriethoxysilane (9 mL, 0.04 mol) was refluxed at 90 °C under a nitrogen atmosphere and for 96 h, after which the crude product was left to cool to room temperature (21 °C). The crude product was then washed with dry diethyl ether (200 mL × 3) and dried at 300 mbar (and at room temperature) to yield the ionic liquid, $[MTESPIm]^+[Cl]^-$. Yield: 10.27 g (53%), ^{1}H NMR (300 MHz, DMSO-d_6) δ 9.35 (s, 1H, NC*H*N), 7.80 (d, J = 6.0 Hz, 2H, NC*H*C*H*N), 4.16 (t, J = 6.5 Hz, 2H, CH_2CH_2N), 3.87 (s, 3H, CHNCH_3), 3.74 (q, J = 6.5 Hz, 6H, CH_3CH_2O), 1.81 (m, 2H, $CH_2CH_2CH_2$), 1.14 (t, J = 6.5 Hz, 9H, CH_3CH_2O), 0.51 (t, J = 6.5 Hz, 2H, $SiCH_2CH_2CH_2$). ^{13}C NMR (75 MHz, DMSO-d_6) δ 136.7 (N*C*HN) 123.6 (N*C*HCHN), 122.2 (NCH*C*HN), 57.8 (CH_2CH_2O), 51.0 (CH_3CH_2N), 35.7 (CHN*C*H_3), 23.7 ($CH_2CH_2CH_2$), 18.2 (CH_3CH_2O), 6.7 ($SiCH_3CH_3$), m/z (ESI) $[M + Na]^+$ 348. Finally, Fe_3O_4@SiO_2 on $[MTESPIm]^+$ $[Cl]^-$ was synthesized following the method of Chen et al. (2014). Briefly, the Fe_3O_4@SiO_2 (1.5 g) was dissolved in toluene (300 mL) and sonicated in an ultrasound bath at room temperature for 10 min. Meanwhile, the ionic liquid (15.40 g) was dissolved in toluene (100 mL) and sonicated at room temperature for 10 min. This ionic liquid solution was then added to the Fe_3O_4@SiO_2 and the mixture was refluxed at 120 °C for 48 h under a nitrogen atmosphere. After 48 h, the reaction mixture was left to cool to room temperature, the solids were separated using an externally applied magnetic field, and the supernatant was decanted. The residual solid was washed with deionized H_2O (250 mL × 2) and ethanol (250 mL × 3) and finally dried at 300 mbar (and 70 °C) to yield Fe_3O_4@SiO_2@$[MTESPIm]^+[Cl]^-$.

Determination of particle diameter

Particle diameter was evaluated using the Scherrer equation as defined below:

$$\tau = \frac{K\lambda}{\beta \mathrm{Cos}\theta},$$

where τ = particle diameter, K = Scherrer constant for spherical particles (0.94), λ = wavelength of X-ray source, θ = Bragg (diffraction) angle of the most intense peak, and β = broadening of half width at maximum intensity (FWHM) of the most intense peak.

Determination of magnetic nanoparticle surface coverage

The surface coverage of magnetic nanoparticle was evaluated using the equation defined below:

$$\text{No.of molecules per nm}^2 = \frac{W \times d_{Fe_3O_4} \times r \times N_A}{M(1-W) \times 3 \times 10^{21}},$$

where W is the weight loss of sample, d_{Fe3O4} is the density of the Fe_3O_4 = 5.17 g/cm^3, N_A is the Avogadro's constant = 6.022×10^{23}, M is the molecular weight of

the ligand, and r is the radius of the composite nanoparticle.

Determination of sorption isotherms

The sorption isotherm governing the removal of Ag^+ was predicted by means of three isotherm models, Langmuir, Freundlich, and Temkin, using data generated from exposing 10 mg of the nanosorbent (Fe_3O_4@SiO_2@[MTESPIm]$^+$[Cl]$^-$) to 10-mL aqueous solutions containing varying Ag^+ concentrations (4 to 90 mgL^{-1}) in 0.023 M $NaNO_3$ at pH 3 for 15 min at room temperature. Equations representing the sorption isotherms are

Langmuir isotherm:

$$\frac{C_e}{Q_e} = \frac{1}{Q_m K_L} + \frac{C_e}{Q_m},$$

where C_e, Q_e, Q_m, and K_L are the equilibrium Ag^+ concentrations (mgL^{-1}), the amount of Ag^+ on the nanosorbent (mgg^{-1}), the maximum capacity of the nanosorbent (mgg^{-1}), and the Langmuir adsorption constant (L/mg), respectively.

Freundlich isotherm:

$$\log Q_e = \log K_F + \frac{1}{n} \log C_e,$$

where Q_e and C_e have been described above and K_F and n are Freundlich constants related to maximum sorption capacity (mg/g) and heterogeneity factor (mg^{-1}).

Temkin isotherm:

$$Q_e = B\ln A_T + B\ln C_e$$

A_T (Lg^{-1}) and B ($Jmol^{-1}$) are Temkin constants related to the binding constant and heat of sorption, respectively.

Ag^+ removal studies

For the control study, a 500-mL aqueous solution containing 1-mgL^{-1} Ag^+ in 0.023-M $NaNO_3$ was prepared from a 500-mgL^{-1} stock solution. Afterwards, 20 mg of Fe_3O_4, Fe_3O_4@SiO_2, and Fe_3O_4@SiO_2@[MTESPIm]$^+$[Cl]$^-$ were each exposed to 10 mL of the Ag^+ aqueous metal solution at pH 1 inside 30-mL plastic screw cap vials. After 45 min, the solids were magnetically separated in about 2 min and the supernatant was removed using a plastic syringe and prepared for metal content determination by ICP-OES. The batch experiments used to investigate the optimum conditions for the selective removal of Ag^+ onto Fe_3O_4@SiO_2@[MTESPIm]$^+$[Cl]$^-$ were conducted by exposing 10 mg of the nanosorbent to a 10-mL aqueous solution containing Cu^{2+}, Ag^+, and Pb^{2+} each at 2 mgL^{-1} in 0.023-M $NaNO_3$ at an initial pH of 3 unless otherwise stated. The pH of the metal aqueous solutions was adjusted to the desired pH using a few drops (typically between 1 and 10) of dilute 0.001-M HNO_3 or NaOH. For initial pH study, pH of adsorbate solution was varied from 1 to 5. For the contact time study, contact time was varied from 0 to 90 min. For nanosorbent dose study, amount of nanosorbent used was varied from 5 to 80 mg. All batch studies were undertaken in triplicates and at room temperature.

The metal removal efficiency was determined by the equation:

$$\%\mathrm{RE} = \frac{C_i - C_f}{C} \times 100,$$

where % RE is percentage removal efficiency and C_i and C_f (in mgL^{-1}) are the initial and final metal ion concentrations, respectively.

The selectivity factor was determined using the following equations (Shamsipur et al. 2014):

$$K_{Ag^+}/_{M^{n+}} = \frac{K_d^{Ag^+}}{K_d^{M^{n+}}},$$

$$K_d = \frac{(C_i - C_f)v}{mC_f}.$$

K_d is distribution ratio, C_i and C_f are initial and final metal ion concentrations, respectively (in mgL^{-1}), v is the volume of aqueous solution in mL, and m is the mass of nanosorbent (in mg).

Ag^+ stripping efficiency studies

For the stripping efficiency study, Ag^+-impregnated Fe_3O_4@SiO_2@[MTESPIm]$^+$[Cl]$^-$ nanosorbents were washed with deionized H_2O and magnetically separated after which it was contacted with 5 mL of stripping agent (HCl, HNO_3 or thiourea) inside screw-capped plastic vials for 1 h. Thereafter, the nanosorbent were magnetically separated and the supernatant stripping agent solution was carefully withdrawn using a plastic

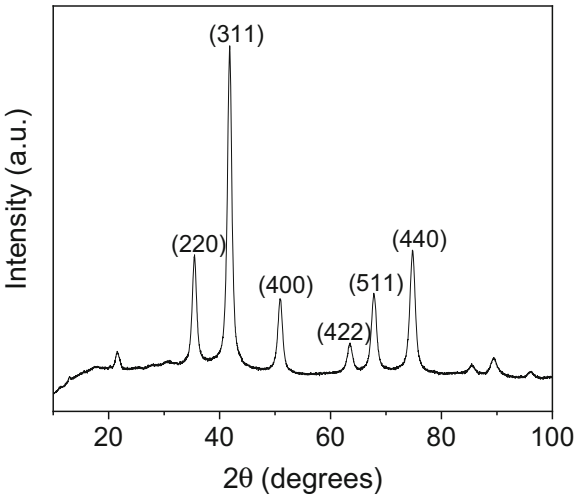

Fig. 2 XRD spectra of Fe_3O_4 nanoparticles (Co Kα source wavelength = 1.790955 Å, voltage = 40 kV, current = 40 mA). The associated d-spacings are 2.96, 2.52, 2.09, 1.71, 1.61, and 1.48 Å for peaks recorded at 2θ: 35.24, 41.58, 50.69, 63.24, 67.57, and 74.52 degrees, respectively

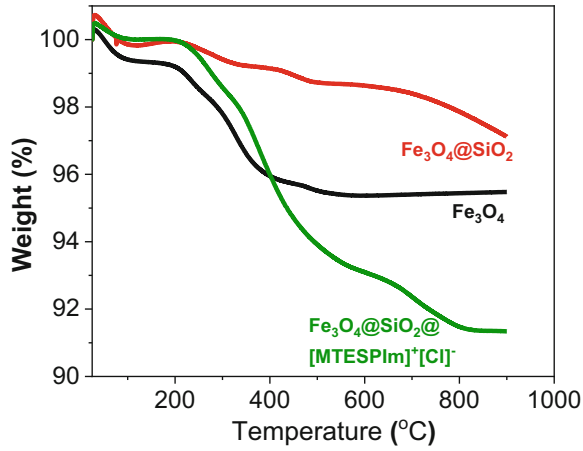

Fig. 4 TGA thermograms for Fe_3O_4 (black), silica-coated Fe_3O_4 (red), and ionic liquid-modified silica-coated Fe_3O_4 nanoparticles (green) (atmosphere, nitrogen; heating rate, 10 °C/min)

syringe. The stripping agent solution was made up to 10 mL by adding deionized H_2O and the metal content was determined again by ICP-OES. The experiments were undertaken in triplicates. The stripping efficiency of Ag^+ by a stripping agent was determined following the equation:

$$\%\mathrm{SE} = \frac{C_e}{C_i} \times 100,$$

where % SE is percentage stripping efficiency, C_e represents the concentration of Ag^+ recovered by the stripping agent (Ag^+ concentration in the stripping agent solution), and C_i represents the initial Ag^+ concentration, respectively (concentration of Ag^+ in nanosorbent prior to stripping).

Results and discussion

Physical and chemical characterization of $[MTESPIm]^+[Cl]^-$ on $Fe_3O_4@SiO_2$

XRD spectra of the black powder obtained after the treatment of $FeSO_4$ and $FeCl_3$ with aqueous ammonia is presented in Fig. 2 and attributed to be that of Fe_3O_4 (Naka et al. 2008; Sun et al. 2007). The average diameter of the Fe_3O_4 particles evaluated by the Scherrer equation (Puig et al. 2012) was found to be 10.0 ± 0.3 nm.

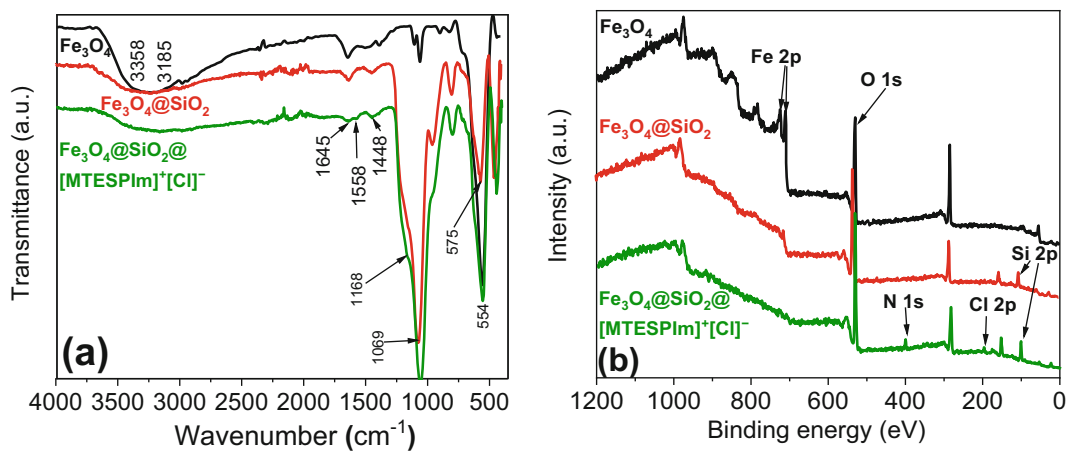

Fig. 3 (**a**) FTIR and (**b**) XPS spectra of Fe_3O_4 (black), $Fe_3O_4@SiO_2$ (red), and $Fe_3O_4@SiO_2@[MTESPIm]^+[Cl]^-$ (green)

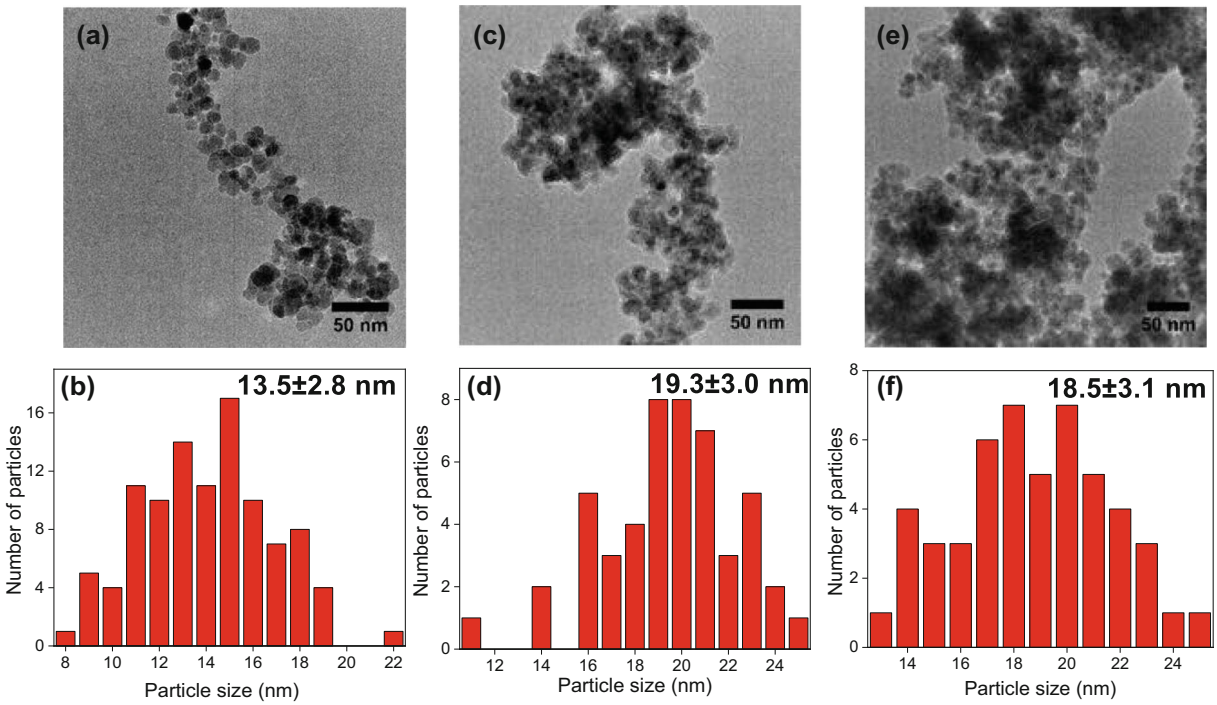

Fig. 5 (a, c, e) Transmission electron micrographs of (**a**) Fe_3O_4, (**c**) silica-coated Fe_3O_4, and (**e**) ionic liquid-modified silica-coated Fe_3O_4 nanoparticles. (b, d, f) Histograms showing size distribution of (**b**) Fe_3O_4, (**d**) silica-coated Fe_3O_4, and (**f**) ionic liquid-modified silica-coated Fe_3O_4 nanoparticles

The chemical compositions of the different nanoparticles synthesized were identified by means of FTIR and XPS. FTIR spectra of all three nanoparticles (Fig. 3a) contain a peak at 554 cm^{-1} which was attributed to the Fe-O vibrations in Fe_3O_4 (Abbas et al. 2014). The peaks in the 1000–1200 cm^{-1} region of the Fe_3O_4 spectrum (Fig. 3a) are attributed to the C-O bonding derived from the residual ethanol that survived the Fe_3O_4 drying. This

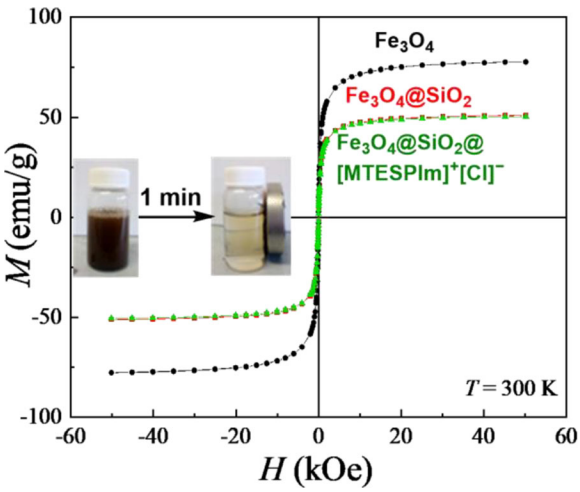

Fig. 6 Magnetization curves for Fe_3O_4 (black), silica-coated Fe_3O_4 (Fe_3O_4@SiO_2) (red), and ionic liquid-modified silica-coated Fe_3O_4 nanoparticles (Fe_3O_4@SiO_2@$[MTESPIm]^+[Cl]^-$) (green) (Inset: separation of Fe_3O_4@SiO_2@$[MTESPIm]^+[Cl]^-$ from deionized water using a magnet)

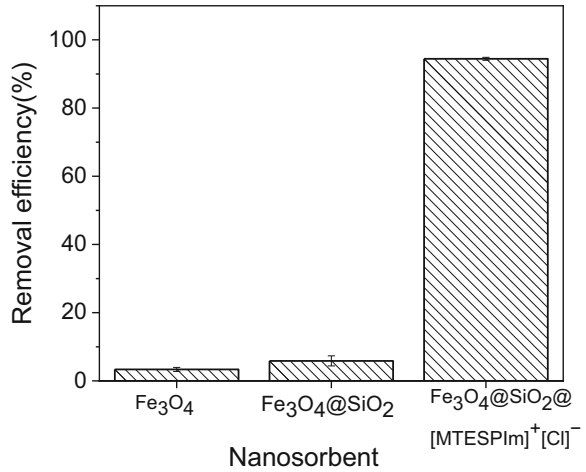

Fig. 7 Extraction efficiencies of Fe_3O_4, silica-coated Fe_3O_4 nanoparticles (Fe_3O_4@SiO_2), and ionic liquid-modified silica-coated Fe_3O_4 nanoparticles (Fe_3O_4@SiO_2@$[MTESPIm]^+[Cl]^-$) for Ag^+ extraction from aqueous solution. (conditions: $[Ag^+]_o = 1\ mgL^{-1}$, volume = 10 mL, pH = 1.0, contact time = 45 min, temperature = RT, nanosorbent dose = 20 mg)

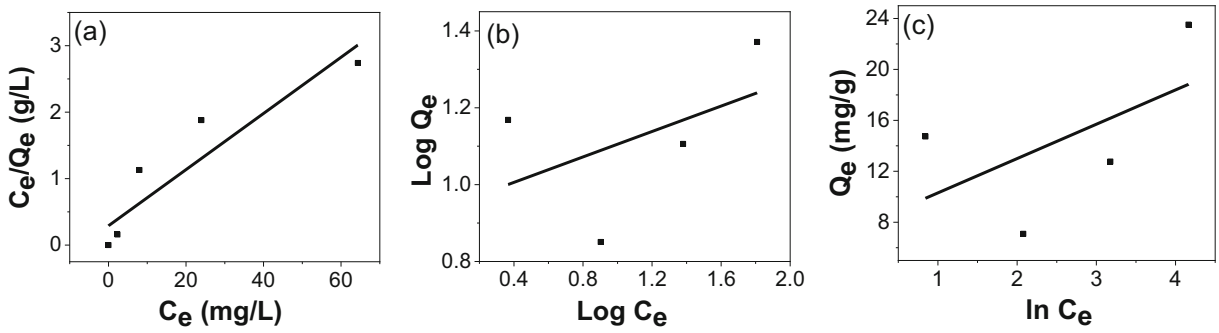

Fig. 8 (**a**) Langmuir, (**b**) Freundlich, and (**c**) Temkin sorption isotherm plots for the removal of Ag^+ by the ionic liquid-modified silica-coated Fe_3O_4 nanosorbent (pH = 3, time = 15 min, nanosorbent dose = 10 mg)

residual solvent was considered of minimal impact on the Fe_3O_4 structure and chemistry because the subsequent SiO_2 coating step was also carried out using ethanol. The spectrum for $Fe_3O_4@SiO_2$ contains an intense peak at 1069 cm^{-1} (attributed to the Si-O-Si stretching vibrations) and suggesting that SiO_2 has been attached to Fe_3O_4 (Abbas et al. 2014; Sajjadifar et al. 2019). While the spectra of the $Fe_3O_4@SiO_2$ and the $Fe_3O_4@SiO_2@[MTESPIm]^+[Cl]^-$ may look identical, the low intensity peak at 1558 cm^{-1} (attributed to the C=N stretching vibration in $[MTESPIm]^+[Cl]^-$) slightly differentiates them, indicating that the ionic liquid ($[MTESPIm]^+[Cl]^-$) may have been linked to the $Fe_3O_4@SiO_2$ (Kim et al. 2007).

XPS spectra (Fig. 3b) corroborates our interpretation of the FTIR data. For example, photoelectron lines representing Fe 2p and O 1 s at 725/710 and 533 eV, respectively, can be observed in the survey spectra of all three nanoparticles (Sun et al. 2007). Furthermore, the spectra of the $Fe_3O_4@SiO_2$ is clearly different from that of the Fe_3O_4 with the presence of the extra photoelectron peak at 106 eV, representing Si 2p and confirming that SiO_2 has been chemisorbed onto the Fe_3O_4. Moreover, the spectra of the $Fe_3O_4@SiO_2@[MTESPIm]^+[Cl]^-$ (Fig. 3b (green)) also contains a photoelectron line corresponding to Si 2p in addition to those at 400, 284.8, and 199 eV which are attributed to N 1s, C 1s, and Cl 2p, respectively. This confirms the chemical bonding of the ionic liquid to the $Fe_3O_4@SiO_2$ (Korin et al. 2017; Sun et al. 2007). Lastly a C 1s photoelectron line was also recorded in all samples at 284.8 eV which is attributed to adventitious carbon (Munho Kim et al. 2017; Miller et al. 2002).

Table 1 Langmuir, Freundlich, and Temkin isotherm parameters for the removal of Ag^+ by the ionic liquid-modified silica-coated Fe_3O_4 nanosorbent ($Fe_3O_4@SiO_2@[MTESPIm]^+[Cl]^-$)

Langmuir			Freundlich			Temkin		
Q_m (mg/g)	K_L (L/mg)	R^2	K_F (mg/g)	n	R^2	B (J/mol)	A_T (L/g)	R^2
23.69	0.15	0.87	8.70	6.04	0.48	2.70	16.80	0.32

The difference in the surface compositions of the nanoparticles was further highlighted by differential weight loss patterns recorded using TGA (Fig. 4). The weight loss of 4% for the Fe_3O_4 nanoparticle between 180 and 570 °C was attributed to the loss of trapped H_2O molecules, residual ethanol in the Fe_3O_4 lattice, and perhaps adventitious carbon as well (Khoobi et al. 2015). As expected, the silica-coated Fe_3O_4 nanoparticles ($Fe_3O_4@SiO_2$) remained stable losing only 3% in the entire experimental temperature range. The ionic liquid-modified silica-coated Fe_3O_4 nanoparticles ($Fe_3O_4@SiO_2@[MTESPIm]^+[Cl]^-$) lost only 9% of their weight, which is attributed to the decomposition of the ionic liquid coating (Xu et al. 2013). The surface coverage of the ionic liquid coating on the $Fe_3O_4@SiO_2$ was determined to be approximately 2 molecules/nm^2.

Analysis using TEM confirm that the Fe_3O_4 are spherical and aggregated with an average particle diameter of (13.5 ± 2.8) nm (Fig. 5 a and b). Such aggregation of bare Fe_3O_4 nanoparticles is not uncommon and attributed to electrostatic and/or magnetic attraction (Ditsch et al. 2005). The difference between the particle diameters obtained using XRD [(10.0 ± 0.3) nm] and micrograph [(13.5 ± 2.8) nm] of Fe_3O_4 was attributed to error associated with manual sizing of the particles from the TEM micrograph. As expected, the $Fe_3O_4@SiO_2$ (Fig. 5c) and $Fe_3O_4@SiO_2@[MTESPIm]^+[Cl]^-$ particles (Fig. 5e) are bigger than the Fe_3O_4 particles with average diameters of 19.3 ± 3.0 (Fig. 5d) and 18.5 ± 3.1 nm (Fig. 5f),

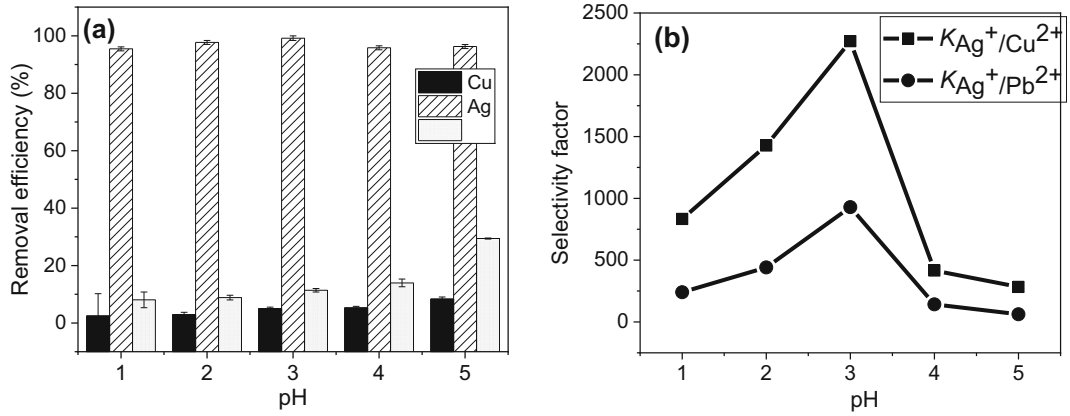

Fig. 9 Effect of pH on (**a**) efficiency and (**b**) selectivity of Ag^+ removal from simulated mixed metal aqueous solution by the ionic liquid-modified silica-coated Fe_3O_4 nanosorbent ($[M^{n+}]$ = 2 mgL^{-1}, volume = 10 mL, contact time = 2 h, temperature = RT, nanosorbent dose = 10 mg)

respectively, noting that these diameters are identical considering their errors. The aggregation observed for the $Fe_3O_4@SiO_2$ (Fig. 5c) particles has been attributed to the increase in ionic strength of the reaction medium as a result of the hydrolysis and condensation of the TEOS (Philipse et al. 1994). On the other hand, aggregation observed for the $Fe_3O_4@SiO_2@[MTESPIm]^+[Cl]^-$ particles (Fig. 5e) may have been caused by intermolecular electrostatic attraction between surfaces bearing the ionic liquid. Based on the diameters of the Fe_3O_4 and the $Fe_3O_4@SiO_2$, the average thickness of the silica layer, which appear as gray fringes in the TEM image (Fig. 5c), is estimated to be approximately 6 nm.

The small particle diameters recorded (all < 20 nm) indicate that all three nanoparticles are likely to be superparamagnetic (Wahajuddin and Arora 2012; Neamtu and Verga 2011). Indeed, this inference was confirmed from the magnetization curves (Fig. 6a) where all three nanoparticles exhibited superparamagnetic behavior (Mahdavian and Mirrahimi 2010; Salviano et al. 2018). Any coercivity is too small to measure and a hysteresis of around ± 20 Oe was observed in the data close to zero magnetization, which is likely to be due to the magnetic field being trapped in the superconducting solenoid. As expected, the Fe_3O_4 has the highest saturation magnetization (M_s) of 77.6 ± 0.1 emu/g. The M_s of the $Fe_3O_4@SiO_2$ and the $Fe_3O_4@SiO_2@[MTESPIm]^+[Cl]^-$ are not significantly different with values of 50.99 ± 0.01 and 50.3 ± 0.1 emu/g respectively, showing that the magnetic response of the $Fe_3O_4@SiO_2$ is not significantly reduced after the surface modification. The lower M_s for $Fe_3O_4@SiO_2$ and $Fe_3O_4@SiO_2@[MTESPIm]^+[Cl]^-$ is

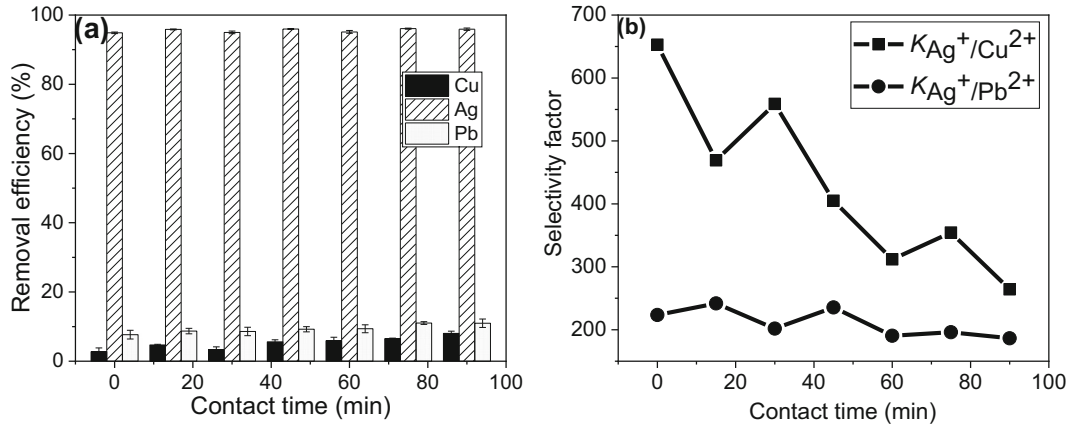

Fig. 10 Effect of contact time on (**a**) efficiency and (**b**) selectivity on Ag^+ removal from simulated mixed metal aqueous solution using the ionic liquid-modified silica-coated Fe_3O_4 nanosorbent (conditions: $[M^{n+}]$ = 2 mgL^{-1}, volume = 10 mL, pH = 1.30, temperature = RT, nanosorbent dose = 10 mg)

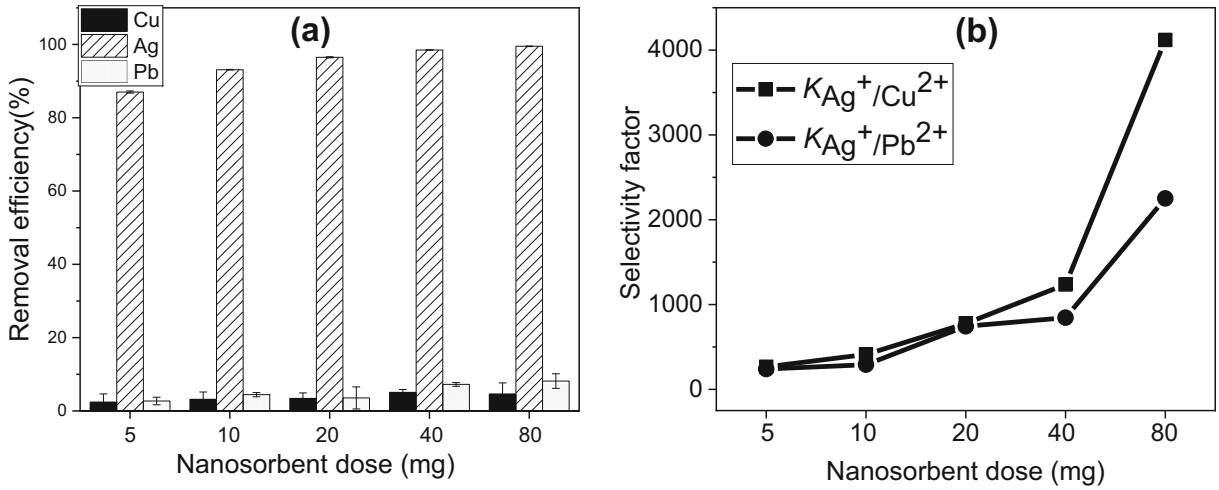

Fig. 11 Effect of nanosorbent dose on (**a**) efficiency and (**b**) selectivity on Ag^+ removal from simulated mixed metal aqueous solution by the nanosorbent $Fe_3O_4@SiO_2@[MTESPIm]^+[Cl]^-$ (conditions: $[M^{n+}] = 2$ mgL^{-1}, volume = 10 mL, pH = 1.30, contact time = 45 min, temperature = RT)

attributed to the surface modifications by nonmagnetic materials, silica and the ionic liquid ($[MTESPIm]^+[Cl]^-$), respectively (Chen et al. 2014). Notwithstanding, the nanoparticle $Fe_3O_4@SiO_2@[MTESPIm]^+[Cl]^-$ can be quickly separated from an aqueous solution in about 1 min (Fig. 6 inset).

Control study

The control study was undertaken to establish the ionic liquid, $[MTESPIm]^+[Cl]^-$, as the agent responsible for the Ag^+ removal. From the control study, it was observed that the Ag^+ removal increased in the order as follows: Fe_3O_4 $[(3.4 \pm 0.6)\%] < Fe_3O_4@SiO_2$ $[(5.8 \pm 1.5)\%] < Fe_3O_4@SiO_2@[MTESPIm]^+[Cl]^-$ $[(94.4 \pm 0.4)\%]$, with $Fe_3O_4@SiO_2@[MTESPIm]^+[Cl]^-$ demonstrating the highest removal efficiency (Fig. 7). The quantitative removal of Ag^+ by the $Fe_3O_4@SiO_2@[MTESPIm]^+[Cl]^-$ may be attributed to the preferential binding of the soft N-donor in the ionic liquid $[MTESPIm]^+[Cl]^-$ to the soft Ag^+ acceptor (Pearson 1968). Going forward, the nanoparticle $Fe_3O_4@SiO_2@[MTESPIm]^+[Cl]^-$ was employed for the investigation of the optimum conditions for the removal of Ag^+.

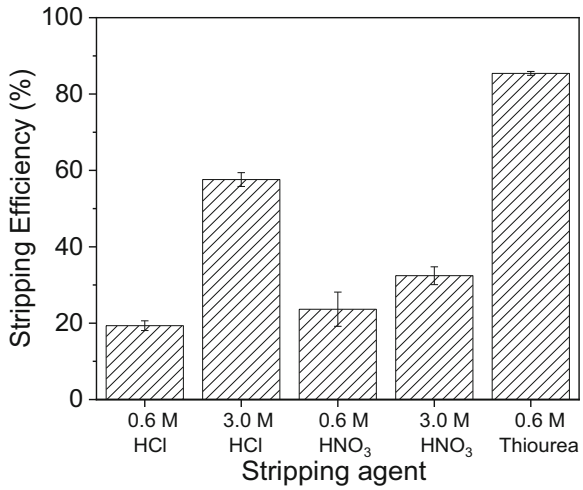

Fig. 12 Relationship between stripping agent type and concentration in the stripping of Ag^+ from impregnated $Fe_3O_4@SiO_2@[MTESPIm]^+[Cl]^-$ nanosorbent (volume of acid = 5 mL, contact time = 1 h, temperature = RT)

Adsorption isotherms

Figures 8 a–c display sorption data plotted against the Langmuir, Freundlich, and Temkin isotherms. The Langmuir isotherm provided the best fit, with an R^2 value of 0.87 compared with 0.48 for Freundlich and 0.32 for Temkin (Table 1). This indicates that Ag^+ removal proceeded predominantly via chemisorption with the formation of a monolayer on $[MTESPIm]^+[Cl]^-$ and with a saturation capacity of 23.69 mg/g. This agrees with Fig. 7 where the removal of Ag^+ onto Fe_3O_4 and $Fe_3O_4@SiO_2$ was comparatively much lower than that observed for $Fe_3O_4@SiO_2@[MTESPIm]^+[Cl]^-$ and therefore suggests that the majority of Ag^+ sorption occurred onto the ionic liquid. This therefore provides strong evidence that $[MTESPIm]^+[Cl]^-$ on $Fe_3O_4@SiO_2$ is a potentially reusable agent for Ag^+ removal.

Effects of initial pH, contact time, and nanosorbent dose on the efficiency and selectivity of removal Ag^+ by the nanosorbent $Fe_3O_4@SiO_2@[MTESPIm]^+[Cl]^-$

The effect of initial pH, contact time, and nanosorbent dose on the removal efficiency and selectivity of the nanosorbent $Fe_3O_4@SiO_2@[MTESPIm]^+[Cl]^-$ for Ag^+ removal in the presence of the competing ions (Cu^{2+} and Pb^{2+}) were investigated by exposing it to aqueous solutions containing low concentrations (ca. 2 mgL^{-1}) of Cu^{2+}, Ag^+, and Pb^{2+}. The choice of Cu^{2+} and Pb^{2+} as competing ions was informed by the knowledge that Ag^+ usually coexists with Cu^{2+} and Pb^{2+} in ores and mine tailings (Crane et al. 2017). Also, low concentrations of Ag^+, Cu^{2+}, and Pb^{2+} were employed in this study because it typically exists in very low concentrations in such repositories of interest.

Effect of initial pH

It was observed that Ag^+ removal efficiency by $Fe_3O_4@SiO_2@[MTESPIm]^+[Cl]^-$ was pH dependent with highest removal (99.2% ± 0.8) observed at pH 3 (Fig. 9a). Quantitative removal of Ag^+ at this pH (pH 3) has been explained by the hard/soft acid/base (HSAB) rule (Pearson 1968). This explanation also helps to understand the quantitative recoveries of Ag^+ at lower pH (pH 1 = 95.5 ± 0.7%; pH 2 = 97.7 ± 0.7%) (Fig. 9a) and also provides clear evidence that $Fe_3O_4@SiO_2@[MTESPIm]^+[Cl]^-$ is stable at such low pH conditions.

Selectivity for Ag^+ over Cu^{2+} and Pb^{2+} by $Fe_3O_4@SiO_2@[MTESPIm]^+[Cl]^-$ was also recorded to be pH dependent, with highest selectivity for Ag^+ (over both Cu^{2+} and Pb^{2+}) observed at pH 3 ($K_{Ag^+/Cu^{2+}}$ = 2272.3 and $K_{Ag^+/Pb^{2+}}$ = 928.7) (Fig. 9b). Selectivity for Cu^{2+} was higher than Pb^{2+} over the pH range investigated, which is counterintuitive given the fact that Cu^{2+} is softer than Pb^{2+}. This is also unlikely to be related to differential precipitation as Pb and Cu chlorides or hydroxides because both are highly soluble at the pH range investigated. It could be related, however, to the average pore size of the nanoparticles (the ionic radius of Pb^{2+} is bigger than Cu^{2+}: 1.27 vs. 0.72 Å), but this hypothesis could not be verified because the pore size of the nanoparticles were not measured.

Effect of contact time

Optimum contact time for Ag^+ removal by $Fe_3O_4@SiO_2@[MTESPIm]^+[Cl]^-$ was investigated by varying the contact time from 0 to 90 min. A duration of 0 min refers to the condition when the nanosorbent is separated immediately after it is exposed to the metal-bearing solution. This magnetic separation process usually takes approximately 60 s.

No significant difference in Ag^+ removal efficacy was recorded for contact times 0–90 min, with the highest and lowest extraction efficiencies being 96.1 ± 0.7% (75 min) and 94.9 ± 0.7% (0 min), respectively (Fig. 10a). This observation was attributed to sufficient availability of surface sites on the nanosorbent, enabling rapid and near-total removal (noting even at 0 min 94.9% of Ag^+ was removed) (Lasheen et al. 2014; Beigzadeh and Moeinpour 2016).

The selectivity factor of Ag^+ over the interfering ions (Cu^{2+} and Pb^{2+}) worsened as a function of the contact time. Highest selectivity for Ag^+ over Cu^{2+} and Pb^{2+} were observed at 0 and 15 min, respectively (Fig. 10b), which suggests that such Ag^+ selective removal is kinetically controlled. The lowest selectivity factor of Ag^+ over Cu^{2+} and Pb^{2+} were observed at 90 min, indicating that exchange of metals between the nanosorbent and the adsorbate may be occurring after the thermodynamic equilibrium has been reached, with the implication that allowance for a lengthy contact time reduces the selective extraction of Ag^+.

Effect of nanosorbent dose

Optimum dose determination is important in order to understand how cost-effective the removal of Ag^+ by $Fe_3O_4@SiO_2@[MTESPIm]^+[Cl]^-$ could be. As expected, Ag^+ removal was recorded to increase with increasing nanosorbent dose (Fig. 11a), namely, 87.0 ± 0.3% at 5 mg and then 99.5 ± 0.1% for 80 mg and attributed to an increase in the number of sorption sites available. Selectivity for Ag^+ over the interfering ions (Cu^{2+} and Pb^{2+}) was also found to be dependent on nanosorbent dose, with highest selectivity recorded for the highest nanosorbent dose tested (80 mg) as follows: $K_{Ag^+/Cu^{2+}}$ = 4119.9 and $K_{Ag^+/Pb^{2+}}$ = 2250.9 (Fig. 11b). The reason for this remains unclear. Therefore, in practical terms, the highest selectivity for Ag^+ can be achieved by using as much of the nanosorbent $Fe_3O_4@SiO_2@[MTESPIm]^+[Cl]^-$ as would be commercially possible.

Effect of type of stripping agents

Efficient recovery of the sorbed metal ion is an important factor to also consider. Therefore, the effect of the type of the stripping agent on the efficiency of Ag^+ recovery was investigated by exposing the aqueous solutions containing Ag^+ sorbed onto $Fe_3O_4@SiO_2@[MTESPIm]^+[Cl]^-$ with three different stripping agents as follows: HCl (0.6 and 3 M), HNO_3 (0.6 and 3 M), and thiourea (0.6 M), noting that 3-M thiourea could not be prepared due to its limited solubility in H_2O. Such stripping agents were selected due to their known thermodynamic efficacy for Ag^+ recovery (Vojoudi et al. 2017; Kazemi et al. 2015; Shimojo and Goto 2004; Abdolmohammad-Zadeh and Javan 2015).

Predictably, the highest percent stripping efficiency (% SE) of 85.4 ± 1.3% was observed for 0.6-M thiourea and this was attributed to the preference of the soft *S*-donor atom in thiourea for the soft Ag^+ acceptor (Fig. 12) (Pearson 1968). HCl (when at 3 M) was recorded to strip more Ag^+ than 3 M HNO_3 (HCl = 59.5 ± 5.5% vs. HNO_3 = 30.9 ± 3.4%), which is likely in part attributed to the formation of the anionic complex $AgCl_2^-$ at high Cl^- concentrations (Abdolmohammad-Zadeh and Javan 2015); however, this difference was not recorded when the acids were applied at 0.6 M.

Conclusion

Surface functionalized magneto-responsive nanoparticles are a new class of materials which have received much interest in recent years for their potential utility as next-generation agents for the recovery of metal(loid)s from the aqueous phase. Herein, $[MTESPIm]^+[Cl]^-$ on $Fe_3O_4@SiO_2$ was prepared and characterized using FTIR, XPS, TGA, TEM, and SQUID, which confirmed that the nanomaterial exhibited a well-constrained composition, physical structure and particle size distribution, in addition to a high saturation magnetism of 50.3 ± 0.1 emu/g which indicates that the nanomaterial is highly amenable for its transport and recovery from the aqueous phase using an externally applied magnetic field. TGA results recorded a surface coverage of $[MTESPIm]^+[Cl]^-$ on the $Fe_3O_4@SiO_2$ of approximately 2 molecules/nm^2. The $[MTESPIm]^+[Cl]^-$ on $Fe_3O_4@SiO_2$ was found to be highly efficient and selective for Ag^+ removal from solutions also containing Cu^{2+} and Pb^{2+}, with optimum efficiency and selectivity recorded at pH 3, with an exposure time of between 0 and 15 min. Fitting of the Langmuir isotherm indicated a monolayer coverage of Ag^+ on the nanosorbent, with a saturation capacity of 23.69 mg/g. Thiourea (0.6 M) was the most effective Ag^+ stripping agent, which is attributed to the preference of the soft *S*-donor atom in thiourea for the soft Ag^+ acceptor. Overall, the results confirm that $[MTESPIm]^+[Cl]^-$ on $Fe_3O_4@SiO_2$ is a highly effective, versatile, and selective agent for the removal of Ag from the aqueous phase and is therefore well suited for multiple future applications in both wastewater treatment and mining sectors.

Funding information The authors would like to thank The UK Commonwealth Scholarship Commission for funding the research under grant number NGCS-2015-448.

Compliance with ethical standards

Conflict of interest The authors declare that they have no conflict of interest.

References

Abbas M, Rao BP, Islam MN, Naga SM, Takahashi M, Kim C (2014) Highly stable-silica encapsulating magnetite nanoparticles (Fe 3O4/SiO2) synthesized using single surfactantless-polyol process. Ceram Int 40(1 PART B):1379–1385. https://doi.org/10.1016/j.ceramint.2013.07.019

Abdolmohammad-Zadeh H, Javan Z (2015) Silica-coated Mn3O4 nanoparticles coated with an ionic liquid for use in solid phase extraction of silver(I) ions prior to their determination by AAS. Microchim Acta 182:1447–1456. https://doi.org/10.1007/s00604-015-1468-x

Ahlatcı F, Koç E, Yazici EY, Celep O, Deveci H (2016) Sulphide precipitation of gold and silver from thiosulphate leach solutions. XV. International Mineral Processing Symposium and Exhibition (IMPS), no. October: 750–60

Avarmaa K, Klemettinen L, O'Brien H, Taskinen P (2019) Urban mining of precious metals via oxidizing copper smelting. Miner Eng 133(January):95–102. https://doi.org/10.1016/j.mineng.2019.01.006

Azgomi N, Mokhtary M (2015) Nano-Fe3O4@SiO2 supported ionic liquid as an efficient catalyst for the synthesis of 1,3-thiazolidin-4-ones under solvent-free conditions. J Mol Catal A Chem 398:58–64. https://doi.org/10.1016/j.molcata.2014.11.018

Banaei A, Vojoudi H, Karimi S, Bahar S, Pourbasheer E (2015) Synthesis and characterization of new modified silica coated magnetite nanoparticles with bisaldehyde as selective adsorbents of Ag(i) from aqueous samples. RSC Adv 5(101): 83304–83313. https://doi.org/10.1039/c5ra11765h

Beigzadeh P, Moeinpour F (2016) Fast and efficient removal of silver (I) from aqueous solutions using aloe Vera Shell ash supported Ni0.5Zn0.5Fe2O4magnetic nanoparticles. Trans Nonferrous Met Soc China (Engl Ed) 26(8):2238–2246. https://doi.org/10.1016/S1003-6326(16)64341-8

Butterman BWC, Hilliard HE (2005) Mineral commodity profiles: silver, Virginia https://pubs.usgs.gov/of/2004/1251/2004-1251.pdf

Chen J, Wang Y, Ding X, Huang Y, Kaijia X (2014) Magnetic solid-phase extraction of proteins based on Hydroxy functional ionic liquid-modified magnetic nanoparticles. Anal Methods 6(20):8358–8367. https://doi.org/10.1039/c4ay01786b

Crane RA, Scott TB (2012) Nanoscale zero-valent iron: future prospects for an emerging water treatment technology. J Hazard Mater 211–212:112–125. https://doi.org/10.1016/j.jhazmat.2011.11.073

Crane RA, Sinnett DE, Cleall PJ, Sapsford DJ (2017) Physicochemical composition of wastes and co-located environmental designations at legacy mine sites in the south west of England and Wales: implications for their resource potential. Resour Conserv Recycl 123:117–134. https://doi.org/10.1016/j.resconrec.2016.08.009

Crane RA, Sapsford DJ, Aderibigbe AD (2019) Applications of engineered nanomaterials in the recovery of metals from wastewater. In: Macaskie LE, Sapsford DJ, Mayes WM (eds) Resource Recovery from Wastes: Towards a Circular Economy. RSC, pp 266–286

Daubinet A, Kaye PT (2002) Designer Ligands. VIII. Thermal and microwave-assisted synthesis of silver(I)-selective ligands. Synth Commun 32(20):3207

Ditsch A, Laibinis PE, Wang DIC, Alan Hatton T (2005) Controlled clustering and enhanced stability of polymer-coated magnetic nanoparticles. Langmuir 21(13):6006–6018. https://doi.org/10.1021/la047057+

Dupont D, Brullot W, Bloemen M, Verbiest T, Binnemans K (2014) Selective uptake of rare earths from aqueous solutions by EDTA-functionalized magnetic and nonmagnetic nanoparticles. ACS Appl Mater Interfaces 6(7):4980–4988. https://doi.org/10.1021/am406027y

Fan L, Song J, Bai W, Wang S, Zeng M, Li X, Yang Z, Li H, Haiwei L (2016) Chelating capture and magnetic removal of non-magnetic heavy metal substances from soil. Sci Rep 6(February):1–9. https://doi.org/10.1038/srep21027

Filippousi M, Angelakeris M, Katsikini M, Paloura E, Efthimiopoulos I, Wang Y, Zamboulis D, Van Tendeloo G (2014) Surfactant effects on the structural and magnetic properties of iron oxide nanoparticles. J Phys Chem C 118(29):16209–16217. https://doi.org/10.1021/jp5037266

Garkoti C, Shabir J, Mozumdar S (2017) An Imidazolium based ionic liquid supported on Fe3O4@SiO2 nanoparticles as an efficient heterogeneous catalyst for N-formylation of amines. New J Chem 41(17):9291–9298. https://doi.org/10.1039/c6nj03985e

Hufschmid R, Hamed A, Matthew Ferguson R, Gonzales M, Teeman E, Brush LN, Browning ND, Krishnan KM (2015) Synthesis of phase-pure and monodisperse iron oxide nanoparticles by thermal decomposition. Nanoscale 7(25):11142–11154. https://doi.org/10.1039/c5nr01651g

Jalilian R, Taheri A (2018) Synthesis and application of a novel core-shell-shell magnetic ion imprinted polymer as a selective adsorbent of trace amounts of silver ions. E-Polymers 18(2):123–134. https://doi.org/10.1515/epoly-2017-0108

Karimi MA, Hatefi-Mehrjardi A, Mohammadi SZ, Mohadesi A, Mazloum-Ardakani M, Kabir AA, Kazemipour M, Afsahi N (2012) Solid phase extraction of trace amounts of silver (I) using dithizone-immobilized alumina-coated magnetite nanoparticles prior to determination by flame atomic absorption spectrometry. Int J Environ Anal Chem 92(12):1325–1340. https://doi.org/10.1080/03067319.2011.563385

Kazemi E, Shabani AMH, Dadfarnia S (2015) Synthesis and characterization of a nanomagnetic ion imprinted polymer for selective extraction of silver ions from aqueous samples. Microchim Acta 182(5–6):1025–1033. https://doi.org/10.1007/s00604-014-1430-3

Khoobi M, Delshad TM, Vosooghi M, Alipour M, Hamadi H, Alipour E, Hamedani MP, Sadat ebrahimi SE, Safaei Z, Foroumadi A, Shafiee A (2015) Polyethyleneimine-modified superparamagnetic Fe3O4 nanoparticles: an efficient, reusable and water tolerance nanocatalyst. J Magn Magn Mater 375:217–226. https://doi.org/10.1016/j.jmmm.2014.09.044

Kim M, Hwang S, Jong Sung Y (2007) Novel ordered Nanoporous graphitic C3N4 as a support for Pt-Ru anode catalyst in direct methanol fuel cell. J Mater Chem 17(17):1656–1659. https://doi.org/10.1039/b702213a

Kim M, Seo JH, Zhao D, Liu SC, Kim K, Lim K, Zhou W, Waks E, Ma Z (2017) Transferrable single crystalline 4H-SiC nanomembranes. J Mater Chem C 5(2):264–268. https://doi.org/10.1039/c6tc04480h

Korin E, Froumin N, Cohen S (2017) Surface analysis of nanocomplexes by X-ray photoelectron spectroscopy (XPS). ACS Biomater Sci Eng 3(6):882–889. https://doi.org/10.1021/acsbiomaterials.7b00040

Lasheen MR, El-Sherif IY, Sabry DY, El-Wakeel ST, El-Shahat MF (2014) Removal and recovery of Cr (VI) by magnetite nanoparticles. Desalin Water Treat 52(34–36):6464–6473. https://doi.org/10.1080/19443994.2013.822158

Mahdavian AR, Mirrahimi MAS (2010) Efficient separation of heavy metal cations by anchoring polyacrylic acid on superparamagnetic magnetite nanoparticles through surface modification. Chem Eng J 159(1–3):264–271. https://doi.org/10.1016/j.cej.2010.02.041

Miller DJ, Biesinger MC, McIntyre NS (2002) Interactions of CO2 and CO at fractional atmosphere pressures with iron and iron oxide surfaces: one possible mechanism for surface contamination? Surf Interface Anal 33:299–305. https://doi.org/10.1002/sia.1188

Naka K, Narita A, Tanaka H, Chujo Y, Morita M, Inubushi T, Nishimura I, Hiruta J, Shibayama H, Koga M, Ishibashi S, Seki J, Kizaka-Kondoh S, Hiraoka M (2008) Biomedical applications of imidazolium cation-modified iron oxide nanoparticles. Polym Adv Technol 19:1421–1429. https://doi.org/10.1002/pat.1218

Neamtu J, Verga N (2011) Magnetic nanoparticles for magneto-resonance imaging and targeted drug delivery. Digest J Nanomater Biostruct 6(3):969–978

Ozkaya T, Baykal A, Kavas H, Köseoğlu Y, Toprak MS (2008) A novel synthetic route to Mn3O4 nanoparticles and their magnetic evaluation. Phys B Condens Matter 403(19–20):3760–3764. https://doi.org/10.1016/j.physb.2008.07.002

Pearson RG (1968) Hard and soft acids and bases, HSAB, part I: fundamental principles. J Chem Educ 45(9):581–587. https://doi.org/10.1021/ed045p581

Philipse AP, Van Bruggen MPB, Pathmamanoharan C (1994) Magnetic silica dispersions: preparation and stability of surface-modified silica particles with a magnetic core. Langmuir 10(1):92–99. https://doi.org/10.1021/la00013a014

Puig J, Hoppe CE, Fasce LA, Pérez CJ, Piñeiro-Redondo Y, Bañobre-López M, López-Quintela MA, Rivas J, Williams RJJ (2012) Superparamagnetic nanocomposites based on the dispersion of oleic acid-stabilized magnetite nanoparticles in a diglycidylether of bisphenol A-based epoxy matrix: magnetic hyperthermia and shape memory. J Phys Chem C 116: 13421–13428. https://doi.org/10.1021/jp3026754

Qian L, Sun J, Hou C, Yang J, Li Y, Lei D, Yang M, Zhang S (2017) Immobilization of BSA on ionic liquid functionalized magnetic Fe3O4 nanoparticles for use in surface imprinting strategy. Talanta 168(January):174–182. https://doi.org/10.1016/j.talanta.2017.03.044

Sahan M, Kucuker MA, Demirel B, Kuchta K, Hursthouse A (2019) Determination of metal content of waste mobile phones and estimation of their recovery potential in Turkey. Int J Environ Res Public Health 16(5). https://doi.org/10.3390/ijerph16050887

Sajjadifar S, Zolfigol MA, Tami F (2019) Application of 1-methyl imidazole-based ionic liquid-stabilized silica-coated Fe 3 O 4 as a novel modified magnetic nanocatalyst for the synthesis of pyrano[2,3-d]pyrimidines. J Chin Chem Soc 66(3):307–315. https://doi.org/10.1002/jccs.201800171

Salviano LB, da Silva Cardoso TM, Silva GC, Dantas MSS, de Mello Ferreira A (2018) Microstructural assessment of magnetite nanoparticles (Fe3O4) obtained by chemical precipitation under different synthesis conditions. Mater Res 21(2):2–8. https://doi.org/10.1590/1980-5373-mr-2017-0764

Seddon KR, Stark A, Torres M-j (2000) Influence of Chloride, water, and organic solvents on the physical properties of ionic liquids. 72(12):2275–2287

Shamsipur M, Hashemi B, Dehdashtian S, Mohammadi M, Gholivand MB, Garau A, Lippolis V (2014) Silver ion imprinted polymer nanobeads based on a Aza-thioether crown containing a 1,10-phenanthroline subunit for solid phase extraction and for voltammetric and potentiometric silver sensors. Anal Chim Acta 852:223–235. https://doi.org/10.1016/j.aca.2014.09.028

Shimojo K, Goto M (2004) Solvent extraction and stripping of silver ions in room-temperature ionic liquids containing calixarenes. Anal Chem 76(17):5039–5044. https://doi.org/10.1021/ac049549x

Sun Y, Ding X, Zheng Z, Xu C, Hu X, Peng Y (2007) Surface initiated ATRP in the synthesis of iron oxide/polystyrene core/shell nanoparticles. Eur Polym J 43:762–772. https://doi.org/10.1016/j.eurpolymj.2006.10.021

Taillades G, Sarradin J (2004) High performance anode for thin film lithium ion batteries. J Power Sources 125(2):199–205. https://doi.org/10.1016/j.jpowsour.2003.07.004

Virolainen S, Tyster M, Haapalainen M, Sainio T (2015) Ion exchange recovery of silver from concentrated base metal-chloride solutions. Hydrometallurgy 152:100–106. https://doi.org/10.1016/j.hydromet.2014.12.011

Vojoudi H, Badiei A, Banaei A, Bahar S, Karimi S, Ziarani GM, Ganjali MR (2017) Extraction of gold, palladium and silver ions using organically modified silica-coated magnetic nanoparticles and silica gel as a sorbent. Microchim Acta 184(10): 3859–3866. https://doi.org/10.1007/s00604-017-2414-x

Wahajuddin A, Arora S (2012) Superparamagnetic iron oxide nanoparticles: magnetic nanoplatforms as drug carriers. Int J Med 7:3445–3471

Wei Y, Li Y, Tian A, Fan Y, Wang X (2013) Ionic liquid modified magnetic microspheres for isolation of heme protein with high binding capacity. J Mater Chem B 1(15):2066–2071. https://doi.org/10.1039/c3tb00576c

Xu J, Caixia J, Sheng J, Wang F, Zhang Q, Sun G, Sun M (2013) Synthesis and characterization of magnetic nanoparticles and its application in lipase immobilization. Bull Kor Chem Soc 34(8):2408–2412. https://doi.org/10.5012/bkcs.2013.34.8.2408

Yang F, Shen R, Long Y, Sun X, Tang F, Cai Q, Yao S (2011) Magnetic microsphere confined ionic liquid as a novel sorbent for the determination of chlorophenols in environmental water samples by liquid chromatography. J Environ Monit 13(2):440–445. https://doi.org/10.1039/c0em00389a

Yin X, Long J, Yu X, Luo X (2017) Recovery of silver from wastewater using a new magnetic photocatalytic ion-imprinted polymer. ACS Sustain Chem Eng 5(3):2090–2097. https://doi.org/10.1021/acssuschemeng.6b01871

Zhou H, Yang L, Li W, Shou Q, Xu P, Li W, Wang F, Yu P, Liu H (2012) Improving the stability of immobilized penicillin G acylase via the modification of supports with ionic liquids. Ind Eng Chem Res 51(12):4582–4590. https://doi.org/10.1021/ie202745c